



Overstory-understory land cover mapping at the watershed scale: accuracy enhancement by multitemporal remote sensing analysis and LiDAR

Laura Fragoso-Campón¹  · Elia Quirós¹  · Julián Mora²  · José Antonio Gutiérrez Gallego¹  · Pablo Durán-Barroso³ 

Received: 19 October 2018 / Accepted: 6 February 2019
© Springer-Verlag GmbH Germany, part of Springer Nature 2019

Abstract

In forested watersheds, density, land cover, and its vertical structure are crucial factors for flood management, ecosystem monitoring, and biomass inventory. Nowadays, producing land cover maps with high accuracy has become a reality with the application of remote sensing techniques, but in some situations, it is not so easy to distinguish between the overstory and understory vegetation with only spectral information. The main goal of this study was to analyze the accuracy enhancement in overstory and understory land cover mapping at the watershed scale when using the data fusion of seasonal and annual time series of Sentinel-2 images complemented with low-density LiDAR and soil and vegetation indices. The study area was composed by two neighboring watersheds in Badajoz province (Spain). The accuracy of land cover classifications was trained in two ways: first, for each season and several soil-vegetation indices; and second, for the annual series and soil-vegetation indices. Next, LiDAR data were included in both analyses by means of a Boolean metric concerning the height. The obtained results showed that the overall accuracy was better with the annual evaluation when only spectral information was used for the classification. Additionally, if LiDAR data were included in the classification (data fusion), the overall accuracies were highly improved, especially in summer and autumn seasons. This improvement can be a significant issue in the analysis of vegetation structure and its spatial distribution as it is decisive for watershed ecosystem management.

Keywords Remote sensing · Sentinel-2A · Forest land cover · Overstory · Understory · Multitemporal analysis · LiDAR · Random forest

Responsible editor: Philippe Garrigues

✉ Laura Fragoso-Campón
laurafragoso@unex.es

Elia Quirós
equiros@unex.es

Julián Mora
jmora@unex.es

José Antonio Gutiérrez Gallego
jagutier@unex.es

Pablo Durán-Barroso
pduranbarroso@unex.es

Introduction

Watersheds, from an environmental point of view, are ecosystems with hydrological, ecological, and environmental functions. They provide a suitable habitat for vegetation and wildlife that, to a greater or lesser extent, have interactions between the physical and biological characteristics of the water. Forest ecosystems can decrease the quantity of rainfall on the soil surface and, at the same time, reduce the runoff due to canopy and forest floor interceptions (Gökbulak et al. 2016). This reduction highly depends, not only on the intensity and quantity of the precipitation, but also on tree density, forest type, and its vertical structure.

One of the main characteristics of Mediterranean forests is the presence of branching formations: trees and shrubs coexisting in the same habitat. The original vegetation of the Mediterranean Iberian watersheds has been reduced in certain circumstances due to two opposing trends in land use:

¹ Department of Graphic Expression, Universidad de Extremadura, 10003 Cáceres, Spain

² Department of Art and Territorial Sciences, Universidad de Extremadura, 10003 Cáceres, Spain

³ Department of Construction, Universidad de Extremadura, 10003 Cáceres, Spain

progressive abandonment of practices in marginal rural areas and land use intensification in more productive areas (Palomo-Campesino et al. 2018).

Overstory is the highest strata of vegetation in a forest, usually forming the canopy and has been largely studied from the perspectives of distribution (Véga et al. 2016; Zhao et al. 2017) and density (González-Ferreiro et al. 2012; Ma et al. 2017). On the other hand, understory vegetation is also an important component in forest ecosystems, not only because of its contributions to forest structure, function, and species composition, but also because of its essential role in supporting wildlife species and ecosystem services (Tuanmu et al. 2010). More specifically, in the Iberian Dehesa, a grazed Mediterranean open woodland, shrub encroachment has been proposed as an effective method to facilitate natural tree regeneration and ensure the sustainability of silvopastoral systems (López-Díaz et al. 2015). As stated in Caballero Díaz et al. (2015), in this Mediterranean environment, this type of understory species plays a crucial role in ecosystem dynamics.

Nevertheless, the analysis of vegetation structure and its spatial distribution is decisive for many other purposes like ecosystem monitoring and biomass inventory (García et al. 2010; García et al. 2017; Latifi et al. 2015; Li et al. 2017; Nizami et al. 2017).

Nowadays, producing land cover maps with high accuracy has become a reality with the application of remote sensing techniques, but on some occasions, it is not so easy to distinguish between the overstory and understory vegetation by only using the spectral information.

There is a wide availability of satellites and sensors that offer a large range of spatial and spectral resolutions. In this field, Landsat imagery, which are available for free and have the longest time series, have been traditionally used because of its ability to discriminate between different types of coverage (eight spectral bands offered) with a good spatial resolution (30 m) (Ahmed et al. 2015; Akike and Samanta 2016; Bolton et al. 2018; Schultz et al. 2016; Zhao et al. 2016). Even so, with the appearance of Sentinel-2 imagery, new studies on land cover mapping can be performed (Ahmed et al. 2015; Godinho et al. 2017; Immitzter et al. 2016; Sánchez Sánchez et al. 2018).

Spectral information can be complemented by using the so-called vegetation indices (VI). These indices support the discrimination of the vegetal cover since they present characteristic values due to the coloration, water content, and photosynthetic action of the plants (Adamu et al. 2018; Godinho et al. 2016; Hill 2013).

Due to the seasonal cycle of the plants and to distinguish the vegetation with a temporal spectral signature, some authors like Gebhardt et al. (2014) and Zhao et al. (2016) showed how global accuracy in land cover mapping could

be improved by the classification of multitemporal series instead of a single date image.

Moreover, and to distinguish between the overstory and understory vegetation, the inclusion of LiDAR data and machine learning techniques in the classification processes have proven to be one of the best improvements (Bork and Su 2007; Erdody and Moskal 2010; García et al. 2011; Mundt et al. 2006; Mutlu et al. 2008). This data fusion takes advantage of the information provided by LiDAR data on the vertical structure of the vegetation, and the capability of multispectral data to capture the horizontal distribution of vegetation as well as to differentiate vegetation types based on their spectral response (García et al. 2011).

More recently, works such as those of Stojanova et al. (2010), Ahmed et al. (2015), and Zald et al. (2016) have proposed the use of LiDAR and multitemporal series of multispectral images for estimating the LiDAR-measured canopy structure using a time series of Landsat imagery. To reduce the costs associated with large-area acquisitions of LiDAR, in these works, the LiDAR data are used only for the definition of sample data, extrapolating the estimation of the forest structure to the whole area covered by the satellite image. As mentioned in Zald et al. (2016), the most important limitation of the methodology is the inability of LiDAR by itself to provide information of map species composition. This restriction also applies to any variable that is only observable with field plot data or other sources of information.

The capacity of LiDAR data to represent the spatial structure of forest stands has been widely validated in this regard and the density of points per square meter is a crucial factor. When studying overstory, densities around 1 points/m² are enough to determine the coverage of the tree stratum (Ma et al. 2017) and, what is more, González-Ferreiro et al. (2012) suggested that, for forest stand variable estimation, density can be reduced to low values of 0.5 points/m² without a significant loss of information. In contrast, there are fewer works that focus on the study of the understory with LiDAR. In this regard, for the correct definition of this low stratum, it is necessary to have a higher density of the LiDAR point cloud than for the overstory, reaching up to 8 points/m² as shown in Estornell et al. (2011) or even more than 13 points/m², as mentioned in Helleesen and Matikainen (2013). In order to counteract the lack of density, other works have proposed to enhance the classification with additional information like high-resolution infrared orthophotography (Riaño et al. 2007) or by supplementing the analysis with a multispectral image of high spatial resolution (García et al. 2011).

The main goal of this study was to analyze the accuracy enhancement in overstory and understory land cover mapping at the watershed scale when using the data fusion of seasonal and annual time series of Sentinel-2 images complemented with LiDAR and soil and vegetation indices.

Materials and methods

Studied area

The study area is composed of two neighboring watersheds in Badajoz province (Spain) of 146 km² and 194 km², respectively (Fig. 1). According to the Spanish Cultivation and Land Use Map (MAPAMA 2018), the watersheds are mainly covered by the following vegetation types: perennial forest wooded with residual conifers at the overstory, and shrubs and herbaceous at the understory level.

The perennial forest wooded of the overstory is mainly composed of holm oaks (*Quercus ilex*), cork oaks (*Quercus suber*), and Eucalyptus (*E. globulus* and *E. camaldulensis*). Regarding the understory, the evergreen shrubs are mainly *Pistacia lentiscus*, *Cistus ladanifer*, and *Retama sphaerocarpa*. On the other hand, the herbaceous vegetation is predominantly located in the Dehesa below the holm oaks and also in agricultural areas. Finally, other covers like rocky outcrops and almost impervious surfaces (like roads and bare soil) are also present in the study area, but with less importance.

Sentinel-2 data

The Sentinel-2 mission is composed of a constellation of two satellites (A and B) that has offered revisits every 10 days since 2015 (A) and 2017 (B), so they have a global revisit of 5 days since they started working together. The Sentinel-2 images offer different spatial resolutions depending on the spectral band considered. Bands B2, B3, B4, and B8 have a resolution of 10 m, while bands B5, B6, B7, B8a, B11, and B12 have a resolution of 20 m. Finally, bands B9 and B10 have a resolution of 60 m.

As shown in Fig. 1, the studied area is located in tile T30STH. In this way, all cloud-free images from April 2017 to April 2018 (20 images) were processed. Moreover, the images were grouped according to their corresponding season: five autumn images, four winter images, five spring images, and six summer images.

In addition to the spectral bands, various vegetation indices (VI) and soil indices (SI) were obtained for each single date image and included as predictors for the improvement of the classification accuracy (Table 1).

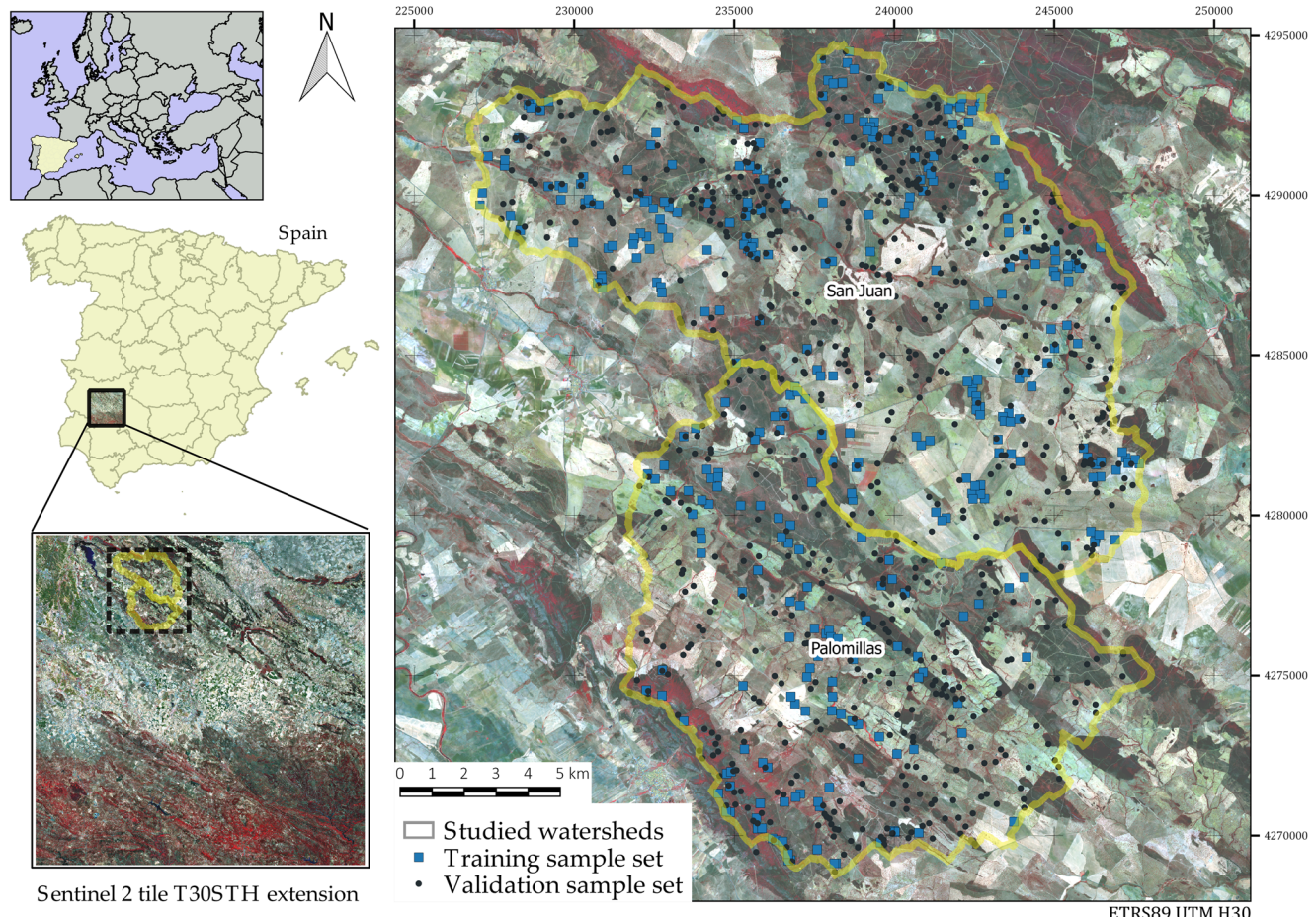


Fig. 1 The two studied watershed in Badajoz province (Spain) represented within the Sentinel-2 tile T30STH (layout in infrared false color). The spatial distribution of the training and validation sample set are also represented

Table 1 Vegetation and soil indices' relation considered in the supervised classification

| Index | Use | Equation |
|---|---|---|
| GNDVI green normalized difference vegetation index | Used to contrast the state of the vegetation between the NIR and the green band | $GNDVI = (B7 - B3)/(B7 + B3)$ |
| NDVI normalized difference vegetation index | Used to measure the photosynthetic activity in correlation with the density and vitality of the vegetation | $NDVI = (B8 - B4)/(B8 + B4)$ |
| NDI45 normalized difference index | Employed to estimate biophysical variables, such as the leaf area index (LAI) | $NDI45 = (B5 - B4)/(B5 + B4)$ |
| S2REP Sentinel-2 Red-Edge Position Index | Includes the information of both crop (chlorophyll content) and growth status of the vegetation | $S2REP = 705 + 35 \times ((B4 + B7)/2 - B5)/(B6 - B5)$ |
| SAVI soil-adjusted vegetation index | Aims at minimizing the effect of the soil on the vegetation indices, especially evident on partially coated surfaces | $SAVI = (1 + L) \times (B8 - B4)/(B8 + B4 + L)$ With $L = 0.5$ |
| MSAVI2 second modified soil-adjusted vegetation index | Similar to the SAVI index, but taking into account that not all soils are alike. Different soils have different reflectance spectra | $MSAVI2 = (1/2) \times (2 \times (B8 + 1) - \sqrt{(2 \times B8 + 1) - 8 \times (B8 - B4)})$ |
| BI brightness index | Uses the albedo of the terrestrial surface to differentiate between the vegetal covers and the ground | $BI = \sqrt{((B4 \times B4) + (B3 \times B3))/2}$ |
| CI color index | Related to the concentration of carbonates or sulfates in the soils | $CI = (B4 - B3)/(B4 + B3)$ |

B_i corresponds with the different spectral bands of the Sentinel-2 images

As shown in Table 1, the VI used were the well-known normalized difference vegetation index (NDVI) originally proposed by Rouse Jr et al. (1974), the soil-adjusted vegetation index (SAVI) developed by Huete (1988) or the second modified soil-adjusted vegetation index (MSAVI2) proposed by Qi et al. (1994), and the green normalized difference vegetation index (GNDVI) developed by Gitelson et al. (1996). Additionally, Sentinel-2 imagery provides more indices rather than the classic ones such as the normalized difference index (NDI45) proposed by Delegido et al. (2011) and the Sentinel-2 Red-Edge Position Index (S2REP), which is based on linear interpolation, as presented by Guyot et al. (1988). In addition, although they are not fully implemented in vegetation classifications yet, soil indices (SI) might be useful to improve the discrimination of low green vegetation canopy covers and the bare soil, as it has been evidenced in Huete et al. (1984) and Richardson and Wiegand (1977). The most extended SI are the brightness index (BI) and the color index (CI) (Escadafal 1993).

LiDAR data

LiDAR data correspond to the National Plan of Aerial Orthophotography (PNOA) of the Spanish National Geographic Institute with a point density of 0.5 points/m², and was acquired in September 2010. The data were downloaded from the Spanish National Geographic Institute website (Instituto-Geográfico-Nacional 2017), who provides it in tiles of 2 km × 2 km. The studied area corresponded to 116 tiles that were analyzed with FUSION software developed by the USDA Forest Service (McGaughey 2009).

The canopy height model (CHM), which represents the digital elevation model of the vegetation above the ground, was processed from the normalized height of the point cloud, creating a raster with pixel cell size of 2 m. The normalization was performed with a ground surface model with a RMSE of 0.114 m. Afterwards, to adjust the CHM to the Sentinel-2 spatial resolution, the raster was processed by generalizing the values to a pixel cell size of 10 m in a similar way to the procedure described in Ahmed et al. (2015). Then, two new rasters were obtained representing the mean and the maximum value in each generalized pixel.

The LiDAR data used is the only one available in Badajoz province up to the present. As a result, there is a time lag between the acquisition of the LiDAR data and the Sentinel images used in this work. Taking into account that the landscape in the studied area is quite stationary, it can be assumed that only phenological changes have occurred during the time lag. However, using a Boolean CHM instead of the physical LiDAR height values would contribute to avoid the noise of the height in low strata caused by the low density of the LiDAR, and to reduce the influence of the evolution in height of the vegetation cover during the time lag. With this regard, the Boolean threshold is crucial to properly define the limit between the overstory and understory, and it needs to be defined analyzing the characteristics of the studied vegetation. As stated before, the evergreen shrubs are composed mainly of *Cistus ladanifer*, whose height ranges from 0.5 to 2.0 m; *Retama sphaerocarpa*, whose height ranges from 0.5 to 3.0 m; and *Pistacia lentiscus*, whose normal height ranges from 1 to 2.0 m. According to these measuring ranges, the limit height in the LiDAR metrics between shrubs and trees was fixed in 3 m above the ground. As a result, both generalized CHM

(mean and maximum values) were transformed into Boolean values: one if LiDAR height was above 3 m and zero if not. These Boolean LiDAR-CHM metrics, unaffected by phenological changes, were included as predictor variables in the classification.

Training and validation areas design

The training and validation samples were defined by photointerpretation over the high spatial resolution (HSR) imagery that also belongs to the National Plan of Aerial Orthophotography (PNOA) of the Spanish National Geographic Institute. In addition, the LiDAR metrics were considered to properly define the sample set. Thus, random stratified training areas were designed following the recommendation of Belgiu and Drăguț (2016). The samples were selected under the criterion of not having suffered significant changes in the time lag between the LiDAR data and the Sentinel imagery. For this purpose, the changes in the vegetation were studied over the available HSR images as near to the date of the LiDAR flight and the date of the Sentinel images as possible. As a result, three series of HSR images were studied: images that date back to 2009 and 2011, those that were taken before and after the LiDAR flight, and the images taken in 2016, which are the most recent ones to the acquisition of the Sentinel images in the studied area.

The land cover classes were grouped by their similar hydrologic response following the criteria of the National Engineering Handbook (NRCS 2009). Therefore, five classes were considered according to their capacity for runoff generation (minor to major): wooded forest (overstory), shrub (understory), herbaceous, and rock (which includes bare soil and impervious areas). Finally, the last class is composed of water bodies which have also been included in the land cover classification.

As a result, 364 sample locations were collected for training. Next, the size of each training area was obtained by expanding the spatial size, depending on the homogeneity around the sample location (Zhao et al. 2016). Finally, the resulting training area was around the 0.69% of the total area (more than 23,400 pixels) (see Fig. 1).

To ensure an objective accuracy assessment, the training and validation areas were designed independently. The appropriate validation sample size was defined using the multinomial distribution, following the guidelines proposed in Congalton and Green (2008) for five land cover classes with a desired confidence level of 95% and a desired precision of 5%. Therefore, 710 random stratified validation samples (cell size of 10 m) were used to generate a valid error matrix. A minimum number of 20 samples were used for water and rock covers due to their very small occupancy.

Supervised classification

The analysis was carried out with the Sentinel Application Platform (SNAP) software developed by the ESA. A pixel-based supervised classification was carried out for land cover mapping by applying the implemented random forest (RF) classifier. The RF classifier (Breiman 2001) is an ensemble classifier that uses a set of classification and regression trees to make a prediction (classification), and works like that by Belgiu and Drăguț (2016) have confirmed that it is suitable for data fusion analysis. When using this classifier, two parameters are decisive to produce the forest trees: the number of decision trees to be generated (Ntree), and the number of variables to be selected and tested for the best split when growing the trees (Mtry). In this work, values of 500 and the square root of the number of input bands were considered respectively. Finally, 5000 pixels per run were considered for the randomization of the training to comply with the principle of the RF classifier.

Seasonal analysis and classification accuracy evaluation

In order to test the effectiveness of the data fusion of LiDAR and the seasonal analysis, the model was trained in two ways. First, the land cover classification was achieved for each season by combining all of the available images for each one as well as considering the VI and SI for each single date image. Second, the land cover classification was carried out for the annual series. Next, LiDAR data were included in the analysis, and as a result, new land cover classifications were achieved both for each season and the annual series. Afterwards, classification accuracies were evaluated by comparing the overall accuracy value derived from the error matrices and by separating differences into two components (quantity and allocation) defined by Pontius and Santacruz (2014). At the same time, the second component was divided into two derived statistics: one is the exchange, which is the component that pairwise confusion causes; and the other one is the shift, which is the one that nonpairwise confusions cause.

The flowchart of the used methodology for land cover mapping is shown in Fig. 2.

Results

Land cover maps obtained from the seasonal analysis are shown in Fig. 3 (autumn), Fig. 4 (winter), Fig. 5 (spring), and Fig. 6 (summer), representing both the considered scenarios of optical data (a), and optical data as well as LiDAR variables (b). Likewise, the results of the annual analysis are shown in Fig. 7.

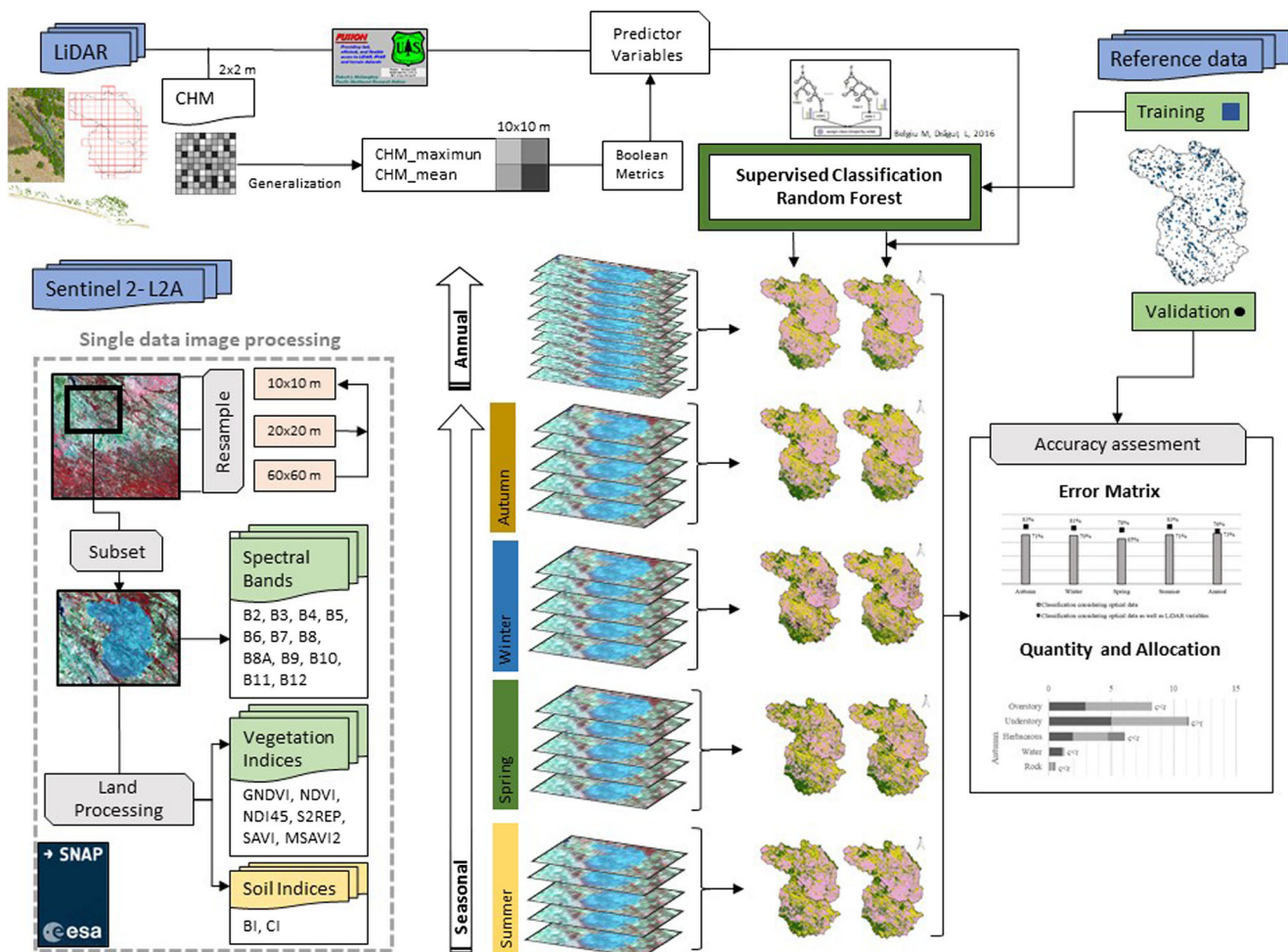


Fig. 2 Flowchart of the methodology used for land cover mapping

Land cover mapping from both the seasonal and annual analyses showed differences in the areal proportion for each cover class. The maximum differences in seasonal analysis were for overstory areas that ranged from 17.16% in winter (Fig. 4b) to 27.69% in spring (Fig. 5a). For understory areas, the differences ranged from 25.88% in summer (Fig. 6b) to 32.82% in autumn (Fig. 3b). For herbaceous areas, the differences ranged from 40.36% in spring (Fig. 5a) to 51.55% in summer (Fig. 6b). For the understory and overstory, a general decrease in the classification area was observed when considering the LiDAR variables; in contrast, the herbaceous classification increased.

The minimum variation between both analyses occurred in the annual one where the overstory areas range only increased from 15.25% (Fig. 7a) to 17.21% (Fig. 7b); the shrub areas slightly increased from 27.07% (Fig. 7a) to 27.77% (Fig. 7b); and the herbaceous areas slightly decreased from 53.84% (Fig. 7a) to 51.20% (Fig. 7b).

For each land cover map, the error matrix was calculated and its corresponding overall accuracy values were compared. According to the results shown in Fig. 8, the annual analysis

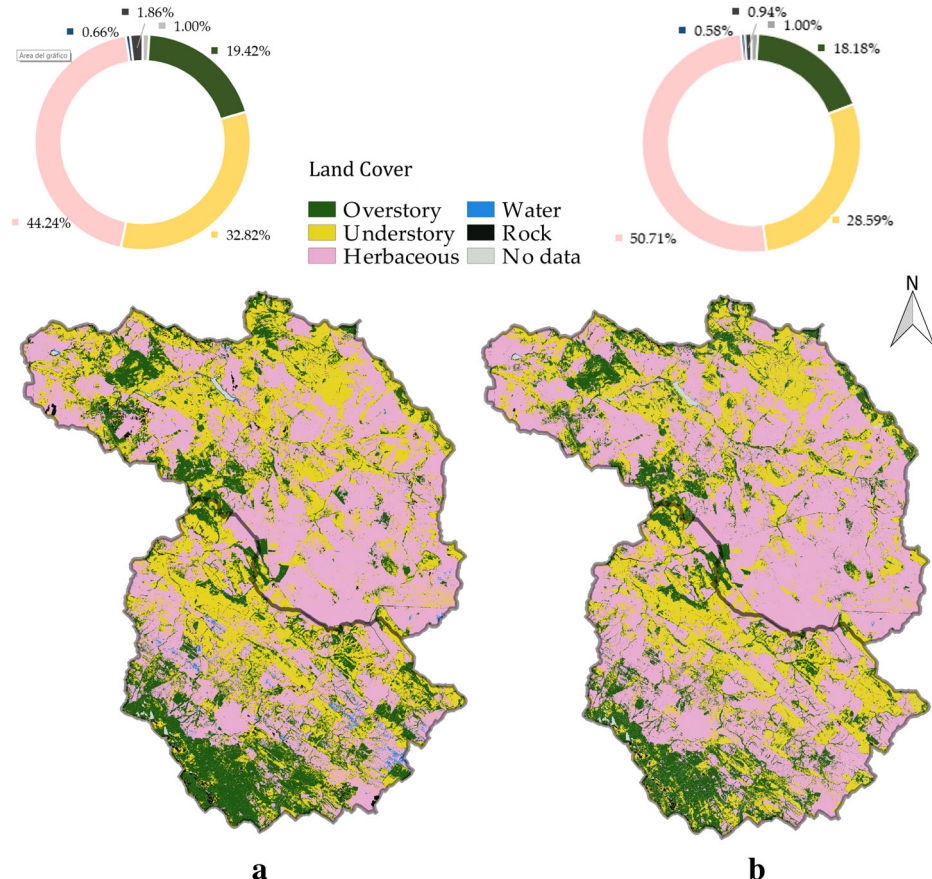
presented a higher accuracy than the seasonal classifications when only the optical data were used. Consequently, the number of images evaluated increased the accuracy of the results. Overall accuracy values ranged from 65% (spring) to 71% (summer and autumn) in the seasonal analysis, but the best value was slightly better for the annual analysis, reaching an overall accuracy of 73%.

In contrast, when the LiDAR data were included in the classification (also shown in Fig. 8), the seasonal overall accuracy has highly improved for every season. The best results were obtained for summer and autumn, where overall accuracy improved from 71 to 83%. In this case, the annual results were only slightly better (from 73 to 76%).

Both the user (Table 2) and producer (Table 3) accuracies performed better when considering the LiDAR data. For the overstory, the best user accuracy values ranged from 72% (spring) to 85% (autumn), and in the case of the understory, these values ranged from 64% (winter and spring) to 71% (autumn).

Additionally, the quantity, exchange, and shift components of each classification, represented in Fig. 9, are in substantial

Fig. 3 Land cover map obtained from the seasonal analysis in autumn representing both the considered scenarios of optical data (**a**), and optical data as well as LiDAR variables (**b**)



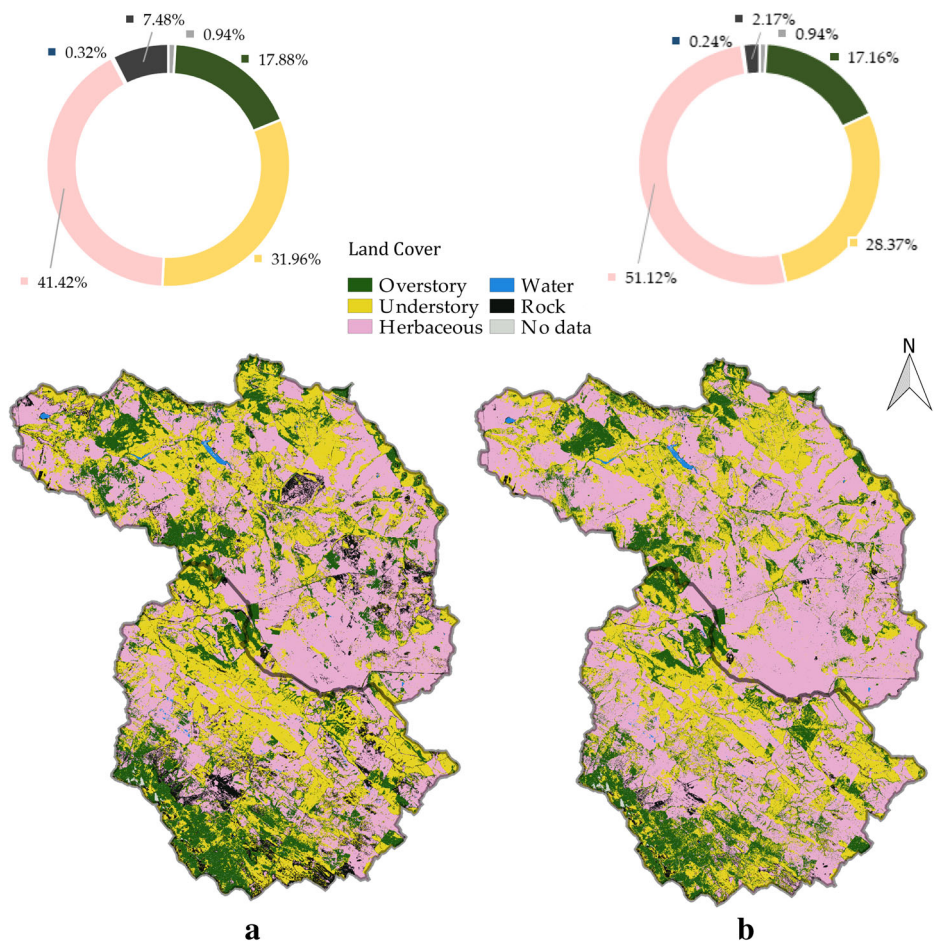
agreement with the more accurate seasons (autumn and summer) and with the increase of OA when LiDAR metrics are included in the classification. Additionally, it can be observed that, in general, the exchange component is greater than the shift component. Therefore, the pairwise confusion is dominant in the classification, but it is considerably reduced when LiDAR variables are included in the classification, especially at the overstory and understory classes.

If the commission disagreement is greater than the omission disagreement for a particular category, the mapped points show more of that category than the reference points, that is the map overestimates the quantity of that category (Gao et al. 2011). This is the case of the understory in all classifications, considering optical data in isolation, or considering optical data in combination with LiDAR variables. As noted above, in this class, a general decrease in the classification area was observed when considering the LiDAR variables, so the overestimation shown in Fig. 9 decreases. On the other hand, if the omission disagreement is greater than the commission disagreement for a particular category, the map underestimates the quantity of that category. In this particular case, we find the herbaceous in all classifications both considering optical data or considering optical data as well as LiDAR variables. As said before, in this class, the classification area increased when

LiDAR metrics were included, so the underestimation shown in Fig. 9 decreases.

As exposed in Breiman (2001), to verify the RF algorithm, after each tree is constructed, the values of each variable in the out-of-bag examples are randomly permuted and the out-of-bag data is run down the corresponding tree. In the SNAP software, each variable is perturbed three times and the percent of correct predictions are averaged, so the importance score is the original percent of correct prediction minus the averaged percent of correct prediction when the variable is permuted. In this way, higher values in the rank suggest that the variable adds information to the algorithm which is significant in the predictive accuracy when combined with the rest of the variables. In this regard, Fig. 10 represents the importance of the predictor variables in the random forest model for the annual evaluation, and Fig. 11 represents the autumn analysis, which is the seasonal analysis that obtained the best results. In both analyses, the bands of near-infrared spectrum (NIR) were significant predictor variables in the evaluation (Fig. 10a and Fig. 11a). In addition, when LiDAR metrics were considered, they were the most important predictors in the classifications (Fig. 10b and Fig. 11b). Figure 11a shows that the bands of NIR B9 and B8 and short-wavelength infrared spectrum (SWIR) bands B11 and B12 were the most

Fig. 4 Land cover map obtained from the seasonal analysis in winter representing both the considered scenarios of optical data (**a**), and optical data as well as LiDAR variables (**b**)



important predictor variables in the evaluation. The soil index CI was ranked in fifth position and finally, with less importance, there were other vegetation indices such as S2REP, MSAVI2, GNDVI, and NDVI. The most representative images were 18-11-2017, 08-12-2017, and 18-12-2017. On the other hand, Fig. 11b shows how the LiDAR metrics were the most important predictor variables, followed by the bands of NIR (B9, B8, and B8a) and SWIR (B11). In this evaluation, the NDVI is ranked sixth and the CI is ranked eighth. The indices SAVI, BI, and NDI45 were given less importance. The most representative images were 09-10-2017, 18-11-2017, 08-12-2017, and 18-12-2017.

Discussion

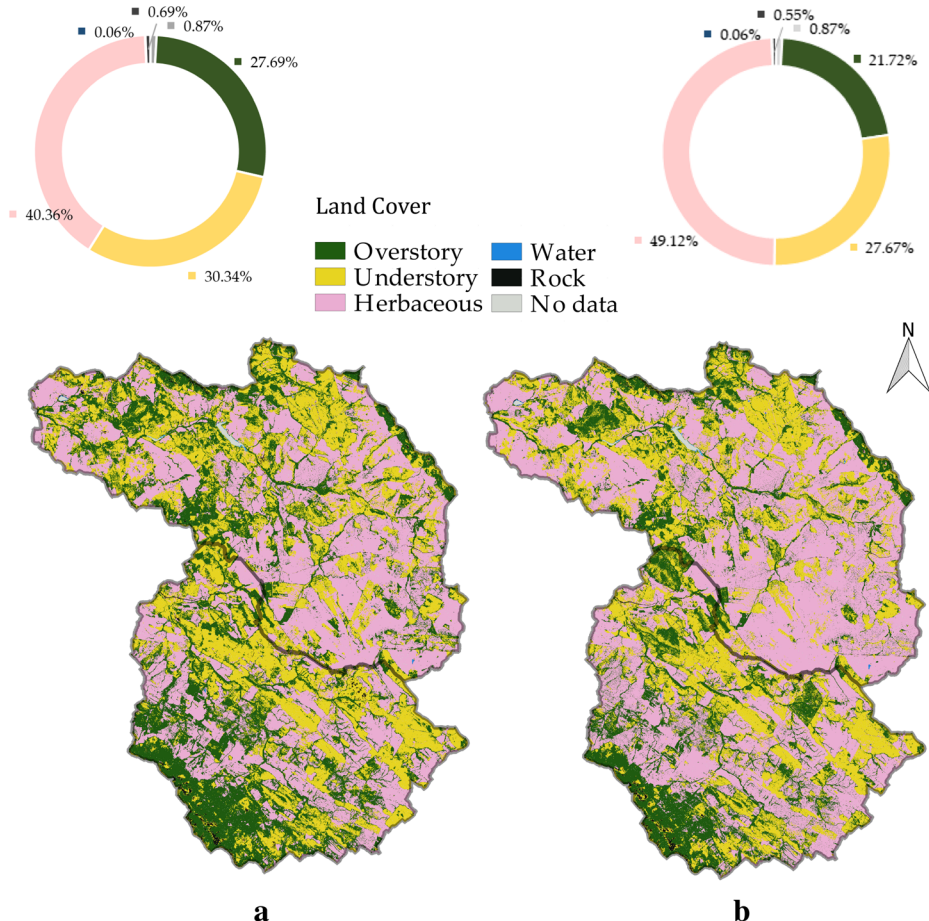
Regarding the OA, the results obtained when exclusively considering the optical data showed that annual imagery classification had the best accuracy, reaching an OA of 73%. This value was in accordance with the results achieved in Gebhardt et al. (2014), which ranged from 70 to 77% in their multitemporal analysis of Landsat imagery and with those

obtained in Zhao et al. (2016), where the OA reached ranged from 73 to 80% with the integration of Landsat multiseasonal data.

On the other hand, when LiDAR data were included in data seasonal classification, the overall accuracy was highly improved for every season in a similar way to that of other previous studies (Ahmed et al. 2015; Erdody and Moskal 2010). The best results were obtained for summer and autumn with an OA of 83%. This value was slightly similar to the results obtained in Sánchez Sánchez et al. (2018) where the OA reached 88% with Sentinel-2 imagery and LiDAR-PNOA data, like in this work. However, this OA was lower than that shown in García et al. (2011) of 94%, although the LiDAR flight had better point density (1.5–6 points/m² higher than the one available and considered in this work of 0.5 points/m²), and additionally, the analysis was performed with a high spatial resolution multispectral image of 2 m, which was also better than the Sentinel-2 spatial resolution of 10 m.

Regarding the seasonal evaluation, the best results reached in autumn could be due to the phenological variability of the vegetation in the studied watershed (perennial forest wooded, shrub, and herbaceous) that showed the best spectral

Fig. 5 Land cover map obtained from the seasonal analysis in spring representing both the considered scenarios of optical data (**a**), and optical data as well as LiDAR variables (**b**)



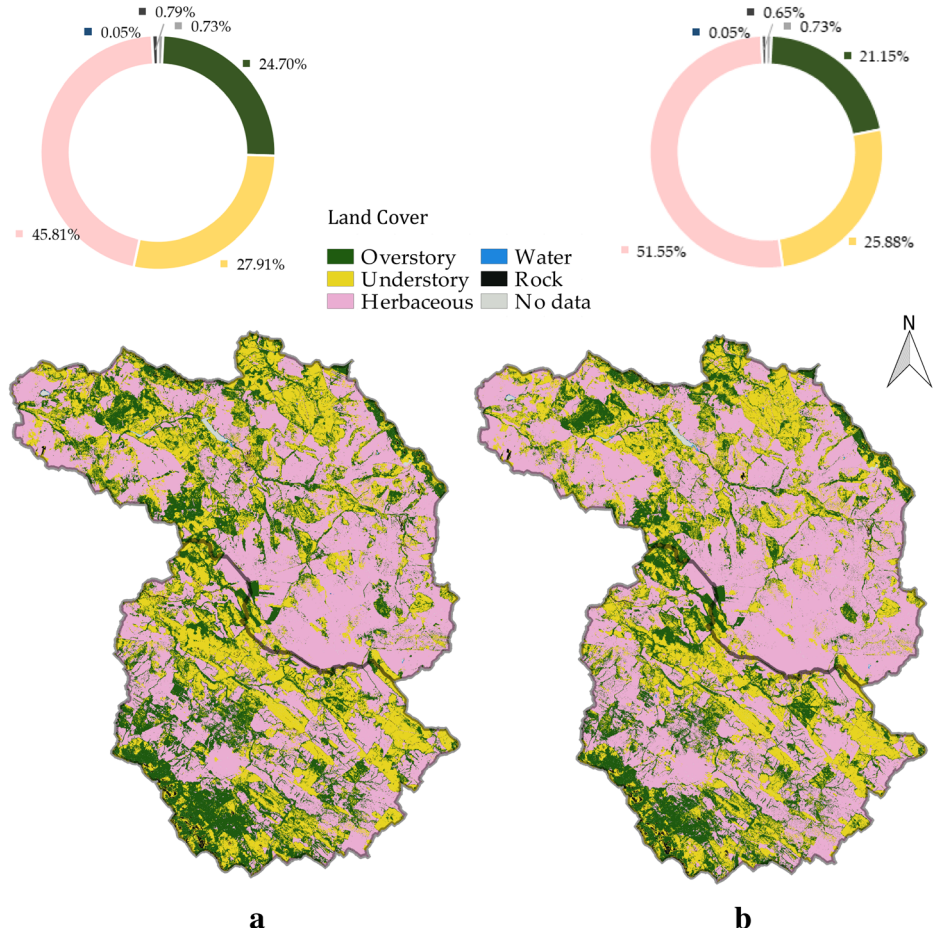
separability in this season. Other single-date studies like Godinho et al. (2016, 2017), and Sánchez Sánchez et al. (2018) selected the image date under this criterion.

In any case, concerning the important predictor variables obtained for the annual analysis when considering only optical data, the most representative were the near-infrared bands and MSAVI2, like the results shown in Vanselow and Samimi (2014), although in this work, only the NDVI was also considered as explanatory variables apart from the RapidEye optical bands. Despite this, the values of the importance score are quite low, ranging from 0.01 to 0.03%, and this is because the annual classification was performed using 380 variables (19 bands in each of the 20 Sentinel images used) and with this great deal of information, there is no specific variable that gives significant information to the classification algorithm. When the LiDAR data is used in the classification, the importance score of the Boolean LiDAR metrics reaches up to 0.16% of score, improving the accuracy of the RF algorithm, more than the rest of the variables. In the same way, in the best seasonal analysis, the bands of NIR and SWIR were the most important predictor variables in the evaluation, with an importance score that ranges from 0.02 to 0.09%. When the LiDAR data is considered in the classification, the importance score of

the Boolean LiDAR metrics reaches up to 1.5%, improving the accuracy of the RF algorithm more than the rest of the variables. This importance score is higher than the annual value because the autumn classification was performed using only 92 variables and the information of the LiDAR metrics has more influence than in the annual analysis.

Considering the user and producer accuracy, the best results were obtained for the scenario with LiDAR data, and showed how, in the case of shrubs, the producer accuracy was over 80% in the best seasonal analysis, similar to the results obtained by Zhao et al. (2016). These understory producer accuracies were even higher than the values obtained for the overstory. Focusing on the quantity and allocation evaluation, the obtained results, when considering optical data as well as LiDAR variables, are significantly better than the ones obtained by Zhou et al. (2014) and by Gao et al. (2011). On the other hand, Gao et al. (2011) attained an overestimation of temperate forest, but no agreement concerning the over or underestimation was found in dry forest. In our work, an overestimation in understory and an underestimation in herbaceous have been achieved in all classifications, but, similarly, no agreement has been obtained for the overstory (forest classes). In particular, understory and herbaceous

Fig. 6 Land cover map obtained from the seasonal analysis in summer representing both the considered scenarios of optical data (**a**), and optical data as well as LiDAR variables (**b**)



classes are both below the limit of the established Boolean threshold, so the LiDAR variables, despite having greatly improved the accuracy of the classification, were not so precise.

Therefore, our results support the conclusions of González-Ferreiro et al. (2012), who considered LiDAR data from the National Plan of Aerial Orthophotography of the Spanish National Geographic Institute as a good source of information for forest management. However, even though the updates of the LiDAR data from the PNOA are not as frequent as desired, it is possible to minimize the effects of the time lag in vegetation heights. Even if the evolution of the vegetation could be despised in the period of the time lag between the LiDAR data and the acquisition of the satellite's images, the lack of accurate height information can be neutralized by applying the Boolean LiDAR metric values as proposed in this work. Nevertheless, the main limitation of this method is that these values might only be applied to separate high and low vegetation, and they probably could not be used to estimate accurate values of forest structure or biomass evaluation. Furthermore, with low-density LiDAR data, the Boolean LiDAR metrics are useful to avoid the noise of the height in low strata. Thus, the confusion produced by the spectral similarities of the understory and overstory vegetation can be

reduced by applying the variables derived from the LiDAR data, which allow for discrimination between the two strata.

Conclusions

In this work, the accuracy enhancement using LiDAR data with Sentinel-2 in multitemporal land cover classification in overstory and understory land cover mapping at the watershed scale was studied. The obtained results showed that the overall accuracies were better with the annual evaluation when only spectral information was used for the classification. Additionally, if LiDAR data were included in the classification (data fusion), the overall accuracies were highly improved, especially in the summer and autumn seasons where those two strata could be more easily differentiated. Thereby, LiDAR data from the National Plan of Aerial Orthophotography of the Spanish National Geographic Institute are a good improvement for data fusion analysis. The proposed methodology based on the use of Boolean LiDAR metrics allows the use of the PNOA LiDAR regardless of the time lag that exists between the LiDAR data and the satellite image acquisition. This improvement can be a

Fig. 7 Land cover map obtained from the annual analysis representing both the considered scenarios of optical data (**a**), and optical data as well as LiDAR variables (**b**)

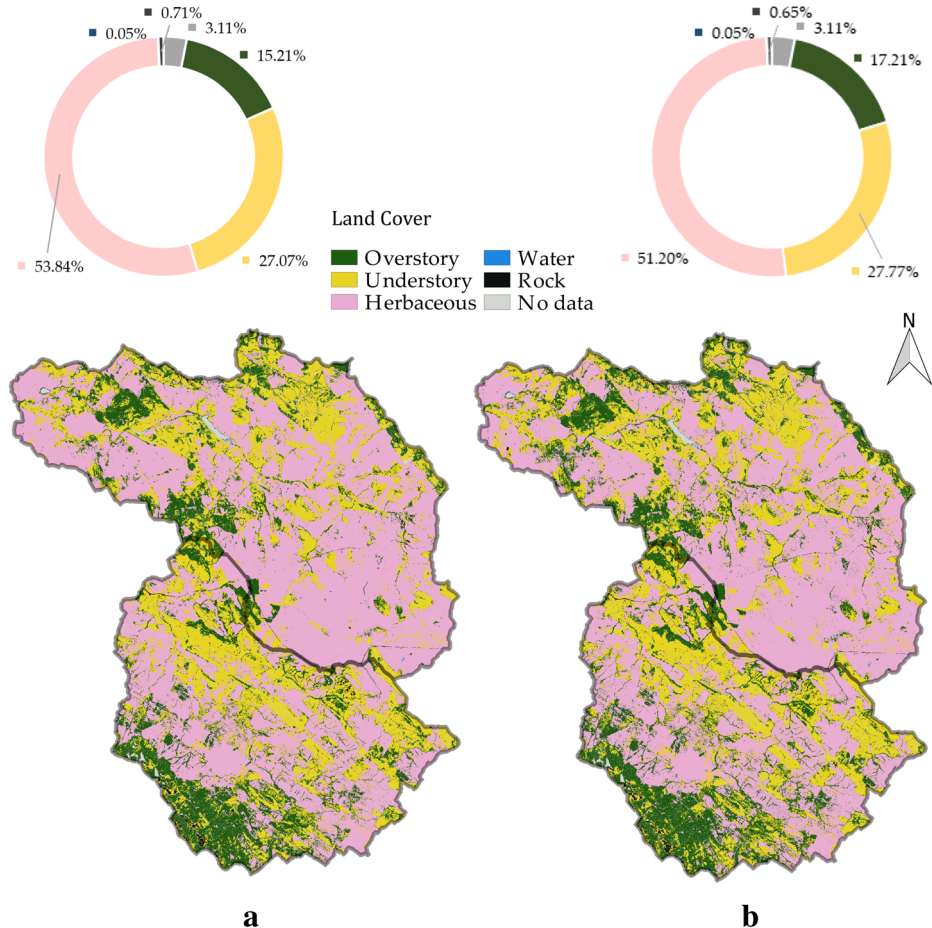


Fig. 8 Overall accuracy (OA) of land cover classifications. The columns represent the OA obtained for each classification considering optical data. The black square plots represent the OA when considering optical data as well as LiDAR variables

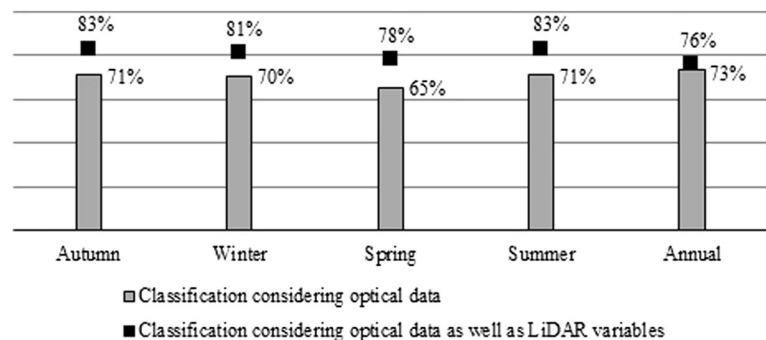


Table 2 User accuracy

| | Classification considering optical data | | | | | Classification considering optical data as well as LiDAR variables | | | | |
|------------|---|------|------|------|------|--|------|------|------|------|
| | Au | Wi | Sp | Su | An | Au | Wi | Sp | Su | An |
| Overstory | 60% | 61% | 54% | 60% | 69% | 85% | 82% | 72% | 84% | 76% |
| Understory | 54% | 54% | 48% | 54% | 59% | 71% | 68% | 64% | 70% | 64% |
| Herbaceous | 96% | 97% | 96% | 96% | 95% | 96% | 95% | 96% | 96% | 96% |
| Water | 67% | 100% | 100% | 100% | 100% | 69% | 100% | 100% | 100% | 100% |
| Rock | 62% | 36% | 100% | 93% | 100% | 75% | 57% | 100% | 94% | 95% |

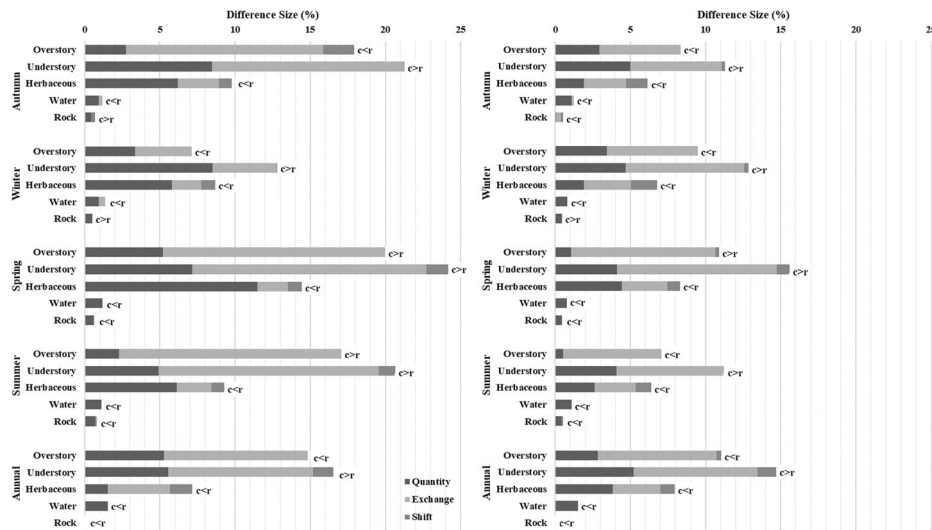
Au, autumn; *Wi*, winter; *Sp*, spring; *Su*, summer; *An*, annual

Table 3 Producer accuracy

| | Classification considering optical data | | | | | Classification considering optical data as well as LiDAR variables | | | | |
|------------|---|-----|-----|-----|-----|--|-----|-----|-----|-----|
| | Au | Wi | Sp | Su | An | Au | Wi | Sp | Su | An |
| Overstory | 51% | 46% | 58% | 61% | 49% | 73% | 68% | 75% | 80% | 63% |
| Understory | 74% | 77% | 69% | 71% | 81% | 87% | 80% | 75% | 86% | 77% |
| Herbaceous | 79% | 76% | 69% | 80% | 90% | 88% | 88% | 85% | 88% | 85% |
| Water | 50% | 70% | 15% | 15% | 40% | 45% | 70% | 15% | 10% | 10% |
| Rock | 90% | 80% | 75% | 70% | 89% | 90% | 85% | 80% | 80% | 90% |

Au, autumn; *Wi*, winter; *Sp*, spring; *Su*, summer; *An*, annual

Fig. 9 Quantity, exchange, and shift components of the classifications. **a** Analysis when considering optical data exclusively and **b** analysis considering optical data as well as LiDAR variables. The label $c < r$ means that the area of the category in the classification is less than the area of the class in the reference (underestimation), and the label $c > r$ means that the area of the category in the classification is greater than the area of the class in the reference (overestimation)



significant issue in the analysis of vegetation structure and its spatial distribution as it is decisive for watershed ecosystem management, flood control, and many other purposes like ecosystem monitoring.

In any case, it must be pointed out that all the data have been obtained from open sources and the calculations have been achieved using free software. Therefore, there are no funding limitations to apply this methodology throughout

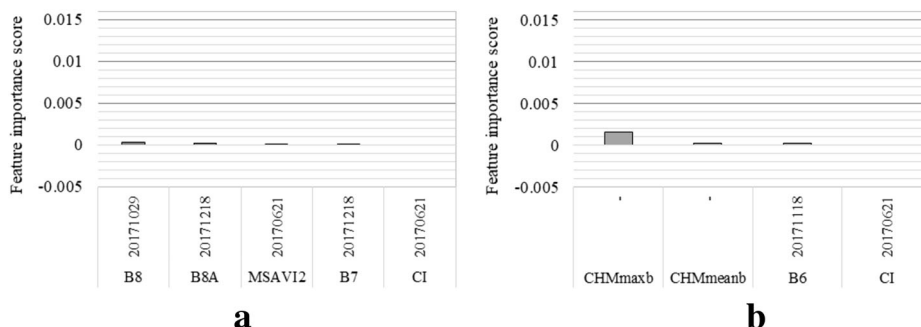
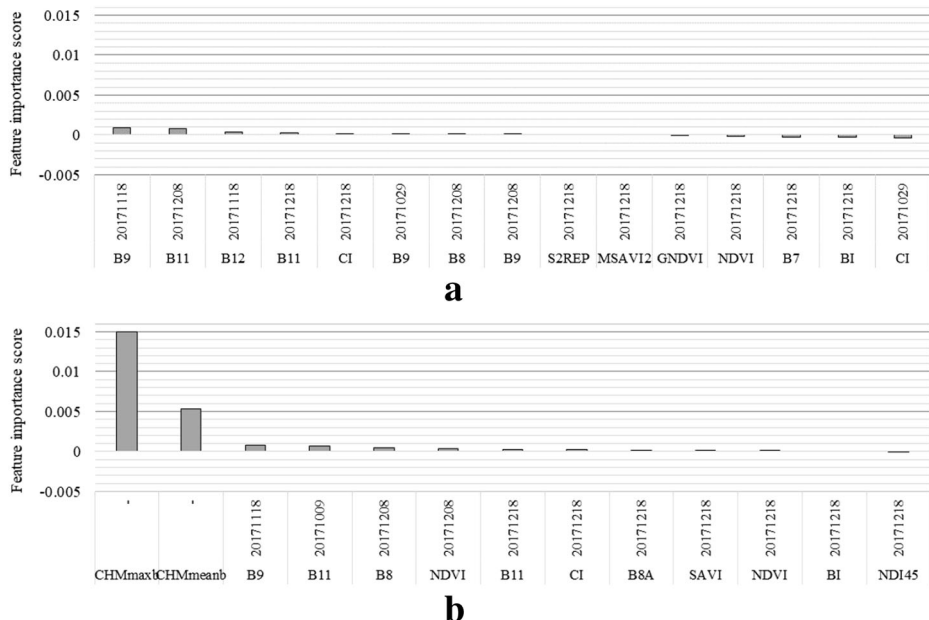


Fig. 10 Predictor variables in annual analysis. Feature importance score obtained in the supervised classification of the land cover applying the Random Forest algorithm. Higher feature importance suggests greater

discriminatory power **a** when considering optical data exclusively and **b** the analysis when considering optical data as well as LiDAR variables

Fig. 11 Predictor variables in seasonal analysis in autumn. Feature importance score obtained in the supervised classification of the land cover applying the Random Forest algorithm. Higher feature importance suggests greater discriminatory power **a** when considering optical data exclusively and **b** when considering optical data as well as LiDAR variables



the Spanish national territory or other regions with uniform LiDAR coverage.

Acknowledgments We thank the Junta de Extremadura (CICTEX) for providing the necessary high-resolution orthophotos PNOA 2007-CC-BY 4.0 scne.es.

Funding information This research was funded by the Junta de Extremadura and the European Social Fund: A way of doing Europe, through the “Financing of Predoctoral Contracts for the Training of Doctors in Public Research and Development Centers belonging to the Extremadura System of Science, Technology, and Innovation [file PD16018]”. This work was also supported by the Government of Extremadura (Spain) and co-funded by the European Regional Development Foundation under Grants [Project: GR18052].

Publisher's note Springer Nature remains neutral with regard to jurisdictional claims in published maps and institutional affiliations.

References

- Adamu B, Tansey K, Ogutu B (2018) Remote sensing for detection and monitoring of vegetation affected by oil spills. *Int J Remote Sens* 39: 3628–3645
- Ahmed OS, Franklin SE, Wulder MA, White JC (2015) Characterizing stand-level forest canopy cover and height using Landsat time series, samples of airborne LiDAR, and the random forest algorithm. *ISPRS J Photogramm Remote Sens* 101:89–101
- Akike S, Samanta S (2016) Land use/land cover and forest canopy density monitoring of Wafi-Golpu project area, Papua New Guinea. *J Geosci Environ Prot* 4:1–14
- Belgiu M, Drăguț L (2016) Random forest in remote sensing: a review of applications and future directions. *ISPRS J Photogramm Remote Sens* 114:24–31
- Bolton DK, White JC, Wulder MA, Coops NC, Hermosilla T, Yuan X (2018) Updating stand-level forest inventories using airborne laser scanning and Landsat time series data. *Int J Appl Earth Obs Geoinf* 66:174–183
- Bork EW, Su JG (2007) Integrating LiDAR data and multispectral imagery for enhanced classification of rangeland vegetation: a meta analysis. *Remote Sens Environ* 111:11–24
- Breiman L (2001) Random forests. *Mach Learn* 45:5–32
- Caballero Díaz J, Pérez F, Manuel A, Quirós Rosado E (2015) A state-and-transition model of Iberian dehesas based on spatial patterns. *For Syst* 24:eRC05. <https://doi.org/10.5424/fs/201524-06408>
- Congalton RG, Green K (2008) Assessing the accuracy of remotely sensed data: principles and practices. CRC press, Boca Raton
- Delegido J, Verrelst J, Alonso L, Moreno J (2011) Evaluation of sentinel-2 red-edge bands for empirical estimation of green LAI and chlorophyll content. *Sensors* 11:7063–7081
- Erdody TL, Moskal LM (2010) Fusion of LiDAR and imagery for estimating forest canopy fuels. *Remote Sens Environ* 114:725–737
- Escadafal R (1993) Remote sensing of soil color: principles and applications. *Remote Sens Rev* 7:261–279
- Estornell J, Ruiz LA, Velázquez-Martí B (2011) Study of shrub cover and height using LiDAR data in a Mediterranean area. *For Sci* 57:171–179
- Gao Y, Marpu P, Niemeyer I, Runfola DM, Giner NM, Hamill T, Pontius RG (2011) Object-based classification with features extracted by a semi-automatic feature extraction algorithm—SEaTH. *Geocarto Int* 26:211–226
- García M, Riaño D, Chuvieco E, Danson FM (2010) Estimating biomass carbon stocks for a Mediterranean forest in central Spain using LiDAR height and intensity data. *Remote Sens Environ* 114:816–830
- García M, Riaño D, Chuvieco E, Salas J, Danson FM (2011) Multispectral and LiDAR data fusion for fuel type mapping using Support Vector Machine and decision rules. *Remote Sens Environ* 115:1369–1379
- García M, Saatchi S, Ferraz A, Silva CA, Ustin S, Koltunov A, Balzter H (2017) Impact of data model and point density on aboveground forest biomass estimation from airborne LiDAR. *Carbon Balance Management* 12(4):4
- Gebhardt S, Wehrmann T, Ruiz M, Maeda P, Bishop J, Schramm M, Kopeinig R, Cartus O, Kellndorfer J, Ressl R, Santos L, Schmidt

- M (2014) MAD-MEX: automatic wall-to-wall land cover monitoring for the Mexican REDD-MRV program using all Landsat data. *Remote Sens* 6:3923–3943
- Gitelson AA, Kaufman YJ, Merzlyak MN (1996) Use of a green channel in remote sensing of global vegetation from EOS-MODIS. *Remote Sens Environ* 58:289–298
- Godinho S, Gil A, Guiomar N, Costa MJ, Neves N (2016) Assessing the role of Mediterranean evergreen oaks canopy cover in land surface albedo and temperature using a remote sensing-based approach. *Appl Geogr* 74:84–94
- Godinho S, Guiomar N, Gil A (2017) Estimating tree canopy cover percentage in a mediterranean silvopastoral systems using Sentinel-2A imagery and the stochastic gradient boosting algorithm. *Int J Remote Sens*:1–23
- Gökbulak F, Şengönül K, Serengil Y, Özhan S, Yurtseven İ, Uygur B, Özçelik MS (2016) Effect of forest thinning on water yield in a sub-humid Mediterranean oak-beech mixed forested watershed. *Water Resour Manag* 30:5039–5049
- González-Ferreiro E, Diéguez-Aranda U, Miranda D (2012) Estimation of stand variables in *Pinus radiata* D. Don plantations using different LiDAR pulse densities. *Forestry* 85:281–292
- Guyot G, Baret F, Major D (1988) High spectral resolution: determination of spectral shifts between the red and the near infrared. *Int Arch Photogramm Remote Sens* 11
- Hellesen T, Matikainen L (2013) An object-based approach for mapping shrub and tree cover on grassland habitats by use of LiDAR and CIR orthoimages. *Remote Sens* 5:558–583
- Hill MJ (2013) Vegetation index suites as indicators of vegetation state in grassland and savanna: an analysis with simulated SENTINEL 2 data for a North American transect. *Remote Sens Environ* 137:94–111
- Huete AR (1988) A soil-adjusted vegetation index (SAVI). *Remote Sens Environ* 25:259–309. [https://doi.org/10.1016/0034-4257\(88\)90106-X](https://doi.org/10.1016/0034-4257(88)90106-X)
- Huete AR, Post DF, Jackson RD (1984) Soil spectral effects on 4-space vegetation discrimination. *Remote Sens Environ* 15(2):155–165. [https://doi.org/10.1016/0034-4257\(84\)90043-9](https://doi.org/10.1016/0034-4257(84)90043-9)
- Immitzer M, Vuolo F, Atzberger C (2016) First experience with Sentinel-2 data for crop and tree species classifications in central Europe. *Remote Sens* 8:166
- Instituto-Geográfico-Nacional (2017) Centro de Descargas. <http://centrodedescargas.cnig.es/CentroDescargas/index.jsp>. Accessed octubre 2017
- Latifi H, Heurich M, Hartig F, Müller J, Krzystek P, Jehl H, Dech S (2015) Estimating over-and understorey canopy density of temperate mixed stands by airborne LiDAR data. *For Int J For Res* 89:69–81
- Li A, Dhakal S, Glenn N, Spaete L, Shinneman D, Pilliod D, Arkle R, McIlroy S (2017) Lidar aboveground vegetation biomass estimates in shrublands: prediction, uncertainties and application to coarser scales. *Remote Sens* 9:903
- López-Díaz M, Rolo V, Benítez R, Moreno G (2015) Shrub encroachment of Iberian dehesas: implications on total forage productivity. *Agrofor Syst* 89:587–598
- Ma Q, Su Y, Guo Q (2017) Comparison of canopy cover estimations from airborne LiDAR, aerial imagery, and satellite imagery. *IEEE J Select Top Appl Earth Observ Remote Sens* 10:4225–4236
- MAPAMA (2018) Mapa de Cultivos y Aprovechamientos de España 2000–2010. http://www.mapama.gob.es/es/cartografia-y-sig/publicaciones/agricultura/mac_2000_2009.aspx. Accessed Enero 2018
- McGaughey RJ (2009) FUSION/LDV: software for LIDAR data analysis and visualization, vol 123. US Department of Agriculture, Forest Service, Pacific Northwest Research Station, Seattle
- Mundt JT, Streutker DR, Glenn NF (2006) Mapping sagebrush distribution using fusion of hyperspectral and lidar classifications. *Photogramm Eng Remote Sens* 72:47–54
- Mutlu M, Popescu SC, Stripling C, Spencer T (2008) Mapping surface fuel models using lidar and multispectral data fusion for fire behavior. *Remote Sens Environ* 112:274–285
- Nizami SM, Yiping Z, Zheng Z, Zhiyun L, Guoping Y, Liqing S (2017) Evaluation of forest structure, biomass and carbon sequestration in subtropical pristine forests of SW China. *Environ Sci Pollut Res* 24: 8137–8146
- NRCS (2009) National Engineering Handbook, section 4, Hydrology, version (1956, 1964, 1971, 1985, 1993, 2004, 2009). National Engineering Handbook. Engineering Division, US. Department of Agriculture, Washington, DC
- Palomo-Campesino S, Ravera F, González JA, García-Llorente M (2018) Exploring current and future situation of Mediterranean silvopastoral systems: case study in Southern Spain. *Rangel Ecol Manag*
- Pontius RG, Santacruz A (2014) Quantity, exchange, and shift components of difference in a square contingency table. *Int J Remote Sens* 35:7543–7554
- Qi J, Chehbouni A, Huete A, Kerr Y, Sorooshian S (1994) A modified soil adjusted vegetation index. *Remote Sens Environ* 48:119–126
- Riaño D, Chuvieco E, Ustin SL, Salas J, Rodríguez-Pérez JR, Ribeiro LM, Viegas DX, Moreno JM, Fernández H (2007) Estimation of shrub height for fuel-type mapping combining airborne LiDAR and simultaneous color infrared ortho imaging. *Int J Wildland Fire* 16: 341–348
- Richardson AJ, Wiegand C (1977) Distinguishing vegetation from soil background information. *Photogramm Eng Remote Sens* 43:1541–1552
- Rouse Jr JW, Haas R, Schell J, Deering D (1974) Monitoring vegetation systems in the Great Plains with ERTS
- Sánchez Sánchez Y, Martínez-Graña A, Santos Francés F, Mateos Picado M (2018) Mapping wildfire ignition probability using sentinel 2 and LiDAR (Jerte Valley, Cáceres, Spain). *Sensors* 18:826
- Schultz M, Clevers JG, Carter S, Verbesselt J, Avitabile V, Quang HV, Herold M (2016) Performance of vegetation indices from Landsat time series in deforestation monitoring. *Int J Appl Earth Obs Geoinf* 52:318–327
- Stojanova D, Panov P, Gjorgjioski V, Kobler A, Džeroski S (2010) Estimating vegetation height and canopy cover from remotely sensed data with machine learning. *Ecol Inform* 5:256–266
- Tuanmu M-N, Viña A, Bearer S, Xu W, Ouyang Z, Zhang H, Liu J (2010) Mapping understory vegetation using phenological characteristics derived from remotely sensed data. *Remote Sens Environ* 114: 1833–1844
- Vanselow KA, Samimi C (2014) Predictive mapping of dwarf shrub vegetation in an arid high mountain ecosystem using remote sensing and random forests. *Remote Sens* 6:6709–6726
- Véga C, Renaud J-P, Durrieu S, Bouvier M (2016) On the interest of penetration depth, canopy area and volume metrics to improve Lidar-based models of forest parameters. *Remote Sens Environ* 175:32–42
- Zald HS, Wulder MA, White JC, Hilker T, Hermosilla T, Hobart GW, Coops NC (2016) Integrating Landsat pixel composites and change metrics with lidar plots to predictively map forest structure and aboveground biomass in Saskatchewan, Canada. *Remote Sens Environ* 176:188–201
- Zhao Y, Feng D, Yu L, Wang X, Chen Y, Bai Y, Hernández HJ, Galleguillos M, Estades C, Biging GS, Radke JD, Gong P (2016) Detailed dynamic land cover mapping of Chile: accuracy improvement by integrating multi-temporal data. *Remote Sens Environ* 183: 170–185
- Zhao Y, Hao Y, Zhen Z, Quan Y (2017) A region-based hierarchical cross-section analysis for individual tree crown delineation using ALS data. *Remote Sens* 9:1084
- Zhou P, Huang J, Pontius RG, Hong H (2014) Land classification and change intensity analysis in a coastal watershed of Southeast China. *Sensors* 14:11640–11658